

Microstructural features affecting the tensile response of Cu-35Cr composites based on crystal-plasticity simulations

Lucas Varoto, Guilhem Martin, Guillaume Hanon, Marc Fivel, Benoit Beausir, Ricardo A Lebensohn, Vincent Taupin

▶ **To cite this version:**

Lucas Varoto, Guilhem Martin, Guillaume Hanon, Marc Fivel, Benoit Beausir, et al.. Microstructural features affecting the tensile response of Cu-35Cr composites based on crystal-plasticity simulations. Mechanics of Materials, 2027, 224, pp.105885. ⟨10.1016/j.mechmat.2026.105885⟩. ⟨hal-05785421⟩

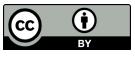
HAL Id: hal-05785421

https://hal.science/hal-05785421v1

Submitted on 8 Oct 2026

HAL is a multi-disciplinary open access archive for the deposit and dissemination of scientific research documents, whether they are published or not. The documents may come from teaching and research institutions in France or abroad, or from public or private research centers.

L'archive ouverte pluridisciplinaire **HAL**, est destinée au dépôt et à la diffusion de documents scientifiques de niveau recherche, publiés ou non, émanant des établissements d'enseignement et de recherche français ou étrangers, des laboratoires publics ou privés.



Distributed under a Creative Commons CC BY 4.0 - Attribution - International License

Mechanics of Materials 224 (2027) 105885

Contents lists available at ScienceDirect

Mechanics of Materials

journal homepage: www.elsevier.com/locate/mechmat

Research paper

Microstructural features affecting the tensile response of Cu-35Cr composites based on crystal-plasticity simulations

Lucas Varoto [a], Guilhem Martin [a,b], Guillaume Hanon [a], Marc Fivel [a], Benoit Beausir [c], Ricardo A. Lebensohn [d], Vincent Taupin [a,*]

[a] Univ. Grenoble Alpes, CNRS, Grenoble INP, SIMaP, Grenoble, F-38000, France
[b] Institut Universitaire de France, F-75005 Paris, France
[c] Université de Lorraine, CNRS, Arts et Métiers, LEM3, Metz, F-57070, France
[d] Theoretical Division, Los Alamos National Laboratory, Los Alamos, NM, 87545, USA

ARTICLE INFO

Handling Editor: Jean-F Molinari

Keywords:
Cu alloys
Microstructure
Mechanical response
Crystal plasticity simulations

ABSTRACT

Cu–Cr-based alloys are promising for thermoelectrical applications owing to their combined electrical, thermal, and mechanical performance. While their electrical properties have been widely explored, their mechanical properties have received much less attention. Herein, we investigate the tensile mechanical response of two Cu-35Cr (%wt) metal matrix composites. The first composite was fabricated by solid state sintering and the other one by vacuum arc remelting. These two processing routes result in significant differences in microstructures. The sintered composite shows equiaxed inclusions of Cr distributed in a Cu matrix with residual pores located within the Cu matrix and at the Cu/Cr interfaces. Its cast counterpart is fully dense (no porosity) and consists of Cr dendrites embedded in a Cu matrix. Monotonic and interrupted tensile tests coupled with EBSD analyses have been conducted. 2D crystal plasticity simulations have been run using the EBSD data collected in the undeformed microstructures as inputs. The model is first validated on the cast material based on the stress-strain tensile response and EBSD measurements performed after different strain increments. Then, we investigate numerically the effect of different microstructural features (initial dislocation density in the Cu matrix, matrix porosity, interfacial porosity, phase fraction, and Cr-phase morphology) on the mechanical response of the sintered composite. The intention is to discriminate the contribution of the different microstructural features on the mechanical response of Cu-Cr composites. This numerical strategy is necessary, because it would be very difficult, if not impossible, to isolate the role of different microstructural features using experiments. We show that the two main contributors to the mechanical response of the sintered composite are the initial dislocation density present in the Cu matrix, and the interfacial pores. On the contrary matrix pores have a minor effect on the mechanical response.

1. Introduction

Cu-Cr composites with a chromium (Cr) content typically exceeding 10 wt% are ideal for use as electrical contacts in vacuum interrupters for medium-voltage applications (Slade, 2020). The electrical contacts must have a combination of high electrical and thermal conductivity, resulting from the highly conductive copper matrix, and good resistance to percussion welding, resulting from chromium reinforcement (Han et al., 2023; Klinski-Wetzel et al., 2015; Von Klinski-Wetzel et al., 2012; Ding et al., 1996; Zhang et al., 2004). These composites play a key role in the power distribution chain, breaking the current in the event of overvoltage or a short circuit (Slade, 2020). They work in the same way as circuit breakers, which are found in every home and are designed to protect electrical devices in the event of a fault in the current flow. Under normal conditions, the electrical contacts are closed, allowing the current to flow. However, if a short circuit occurs, the contacts separate and the current is cut off immediately. Cu-Cr materials are essential for the electrification of modern societies and for reducing reliance on fossil fuels.

Two processing routes have been developed for producing copper-chromium (Cu-Cr) composites on an industrial scale: casting techniques, such as vacuum arc remelting (VAR) (Han et al., 2023; Zhang

* Corresponding author.
E-mail address: vincent.taupin@cnrs.fr (V. Taupin).

https://doi.org/10.1016/j.mechmat.2026.105885
Received 25 June 2026; Received in revised form 9 September 2026; Accepted 30 September 2026
Available online 6 October 2026
0167-6636/© 2026 The Authors. Published by Elsevier Ltd. This is an open access article under the CC BY license (http://creativecommons.org/licenses/by/4.0/).

et al., 2004), and powder metallurgy via solid-state sintering (SSS) (Klinski-Wetzel et al., 2015; Spaić et al., 1989). SSS is often considered as the most cost-effective among the two processes since it does not require as many fabrication steps: there is no need to produce ingots prior to vacuum arc remelting, and machining operations are limited (near-net shape). These two processes result in microstructures that differ drastically in their main characteristics, which are summarized below. The microstructure of Cu-Cr alloys fabricated by VAR with hypereutectic compositions consists of Cr dendrites dispersed in a eutectic matrix that is predominantly made of Cu (Han et al., 2023; Zhang et al., 2004; Varoto et al., 2024). This microstructure does not contain solidification defects, such as shrinkage porosity. In contrast, the microstructure resulting from powder metallurgy consists of Cr particles whose size and morphology depend directly on the powder batch used to produce the near-net-shape electrical contacts (Spaić et al., 1989; Varoto et al., 2023). Densification of the composite occurs upon sintering, but is incomplete. Typically, a relative density of 96–97% is achieved after optimization of the sintering process (Varoto et al., 2023, 2025; Papillon et al., 2017). Consequently, the final components contain residual porosity in the form of spherical pores within the Cu matrix and larger, interconnected pores surrounding the Cr particles (Varoto et al., 2023). These differences in microstructure lead to different mechanical responses and thus properties (Varoto et al., 2024, 2025). In a recent work, we use a full-field modeling approach to investigate, discuss, and assess the effects of different microstructural features such as pores, composition of the Cu matrix, and interfacial thermal resistance, on the effective thermal conductivity of sintered Cu-25Cr composites (Varoto et al., 2025). Interfacial pores, trace elements in solid-solution in Cu matrix, interfacial thermal resistance and the heterogeneous distribution of Cr in the Cu matrix were identified as features governing the effective thermal conductivity of Cu-25Cr sintered composites (Varoto et al., 2025).

In this work, we propose to investigate and discriminate the effect of different microstructural characteristics on the mechanical response of Cu-35Cr composites fabricated by VAR and SSS. Designing and conducting a set of experiments dedicated to the investigation of the sole effect of each microstructural characteristics (e.g. pores, dislocation density and phase fraction) on the mechanical response of Cu-Cr composites would have been highly challenging. For example, it would be very difficult to produce fully dense samples using SSS. It would also be complicated to obtain a unique pore population, for example by removing only the matrix pores while preserving the interfacial pores, or vice versa. To circumvent these experimental difficulties, here we use a modelling-based approach to identify the microstructural characteristics that influence the mechanical response of VAR and SSS Cu-35Cr composites. To this end, we performed 2D crystal plasticity (CP) simulations using a full-field approach based on an elasto-viscoplastic (EVP) model employing fast Fourier transform (FFT) algorithm (EVP-FFT) (Moulinec and Suquet, 1998; Lebensohn et al., 2012; Lebensohn and Needleman, 2016). CP-FFT frameworks have been applied to metal matrix composites, like Cu-Ag systems (Jia et al., 2013; Roters et al., 2019), Cu-Nb nanolaminates (Zecevic et al., 2023), or ceramic particle reinforced ferrite (Genée et al., 2020). In this study, we first determine the tensile mechanical response of Cu-35Cr composites and investigate the evolution of their microstructure during the first 6% of straining using interrupted tensile tests and EBSD analyses. EVP-FFT calculations are then employed to model the mechanical response of the Cu-35Cr composites and calibrated based on the experimental results. Once calibrated, the model is used to investigate the role of various microstructural parameters on the mechanical response of Cu-35Cr composites.

2. Materials and methods

2.1. Materials

Solid state sintered Cu-35Cr composites were supplied by Schneider Electric, Grenoble, France. Cu-35Cr samples produced by VAR were supplied by Sirui Advanced Materials Co., Ltd, Xi'an, China. These two processing routes result in different microstructures which are described in the experimental results section.

2.2. Mechanical testing

Flat dog-bone tensile specimens (gauge length 15 mm, width 3 mm, thickness 1.5 mm) were obtained from the as-received Cu-35Cr SSS and VAR composites using wire-based electron discharge machining (EDM). The surface of the tensile specimens was then carefully grounded using 4000 grit SiC abrasive paper to remove the EDM-affected surface. Both monotonic and interrupted tensile tests were performed using an MTS 4M machine equipped with a 20 kN load cell at a constant strain rate of 0.001 s^{-1}. Monotonic tensile tests were performed to failure. Complementary interrupted tensile tests were performed to monitor the same region of interest after different strain increments (2, 4 and 6% tensile strain). The specimen was unloaded immediately after reaching the desired tensile strain increment to allow microstructural observation of the same region of interest and then reloaded to the next strain increment. Strain measurements were performed using Digital Image Correlation (DIC) with the GOM Metrology Suite software.

2.3. Microstructure observations

Prior to the tensile tests, the specimens were grounded to 4000 grit and polished with diamond suspensions (9, 3 and 1 μm). Finally, the surface of the specimens was prepared by vibratory polishing with a solution of 0.03 μm SiO_2 for at least 4 h. This surface preparation is suitable for SEM imaging and EBSD measurements.

Regions of interest located in the center of the gauge length of the tensile specimens were selected to acquire SEM images using backscattered electron contrast and EBSD maps after different strain increments. SEM imaging and EBSD measurements were performed using a Zeiss Gemini SEM500 scanning electron microscope equipped with an EBSD camera from EDAX. BSE images were acquired using an acceleration voltage of 15 kV and the high current mode. EBSD maps were systematically collected at 20 kV with a step size of 0.5 μm. These maps were post-processed using MTEX. Kernel Average Misorientation (KAM) maps were calculated taking into account all points in the kernel and the first 5 nearest neighbours. The disorientation distributions calculated from the KAM maps were plotted after each strain increment to evaluate its evolution with the tensile strain.

3. Experimental results

3.1. Undeformed microstructures

The microstructures of the Cu-35Cr composites produced by VAR and SSS are shown in Fig. 1b and c respectively. The VAR microstructure is typical of a hypereutectic alloy with Cr-dendrites embedded in the Cu matrix. The characteristic size of the Cr dendrites, estimated by the intercept method, is approximately 10 μm. No pores can be detected. In the SSS Cu-35Cr composite, the Cr phase is drastically different both in size (50 μm, measured by the intercept method) and morphology (equiaxed). This is consistent with the processing route, as the SSS composites were prepared by mixing Cu powder (40 μm) and Cr powder (30-80 μm) in a 65:35% mass ratio. Another striking difference is the presence of residual pores resulting from sintering. The pores can be classified into two families: the fine rounded pores found in the Cu phase, referred to as 'matrix porosity' and pointed with a green arrow in

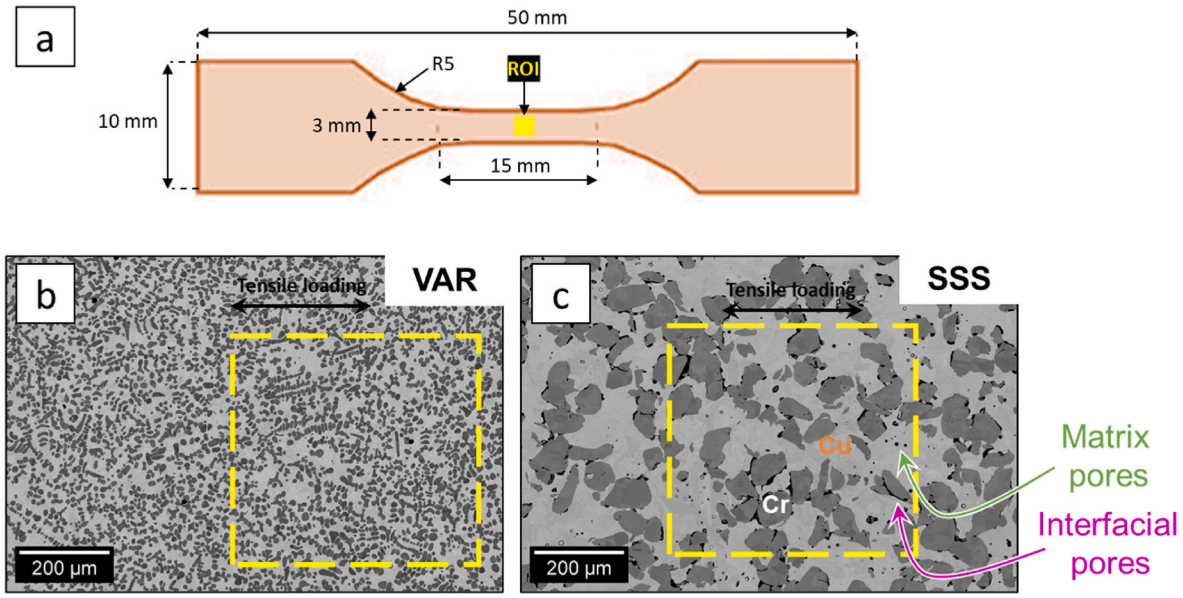


Fig. 1. (a) Geometry of the tensile specimen showing the position of the region of interest along the gauge length selected for the combined EBSD-CPFFT investigations. SEM BSE images of the Cu-35Cr composite fabricated by (b) vacuum arc remelting (VAR) and (c) solid state sintering (SSS) in their undeformed condition. The areas highlighted using dashed yellow lines correspond to the region of interest mapped using EBSD before and after tensile straining. The tensile direction is also indicated.

Fig. 1c, and the 'interfacial porosity' pointed with a pink arrow in Fig. 1c, located at the Cu/Cr interfaces, which are larger in size and have a more complex morphology. The final relative density of the SSS sample, measured by the Archimede method, was 96%. For a detailed 3D characterization of the pore population in the SSS microstructure, the reader is referred to our previous works (Varoto et al., 2023, 2024). It was found that the interfacial porosity represents nearly 90% of the total porosity and that 90% of the Cr particles have an interfacial pore in their vicinity (Varoto et al., 2023, 2025). In addition, interfacial pores often envelop Cr particles and are interconnected in 3D, thus forming a network of interfacial porosity (Varoto et al., 2023).

The areas highlighted with yellow dashed lines in Fig. 1b and c correspond to the regions of interest mapped by EBSD in the undeformed state and after different tensile strain increments. The copper grain size, measured by EBSD and defined as the equivalent diameter, is about 25 ± 10 µm in the SSS composite and 15 ± 10 µm in the VAR composite. The KAM maps of the Cu and Cr phases in the undeformed microstructure of the VAR and SSS composites are shown in Fig. 2a and b and Fig. 2c and d respectively. The average disorientation in the Cu phase calculated from the KAM maps is higher (1.3°) in the VAR than in the SSS (0.8°). In the Cr phase, the average KAM in the VAR (1.2°) is twice of that in SSS (0.6°). However, evaluating the average KAM alone does not allow one to assess the heterogeneity in local disorientation. Examination of the KAM maps reveals that the KAM in the Cr phase of the VAR composite is more heterogeneously distributed than within the Cu phase (Fig. 2a–c). In the Cr phase, some regions show a disorientation $<1°$ (in dark blue) while other exhibit disorientation approaching 5° (in red). Overall, higher disorientations are observed in the Cr phase of the VAR composite compared to that of the SSS. All these observations are further supported by looking at the local disorientation distributions in each phase, see Fig. 2e and f. For example, the regions with the largest disorientation are predominantly found in the Cr phase in the VAR composite, while they are preferentially located in the Cu phase in the SSS material. In the latter, the regions with the largest disorientation are always found in narrow Cu regions confined between Cr particles.

Assuming that the KAM distribution can be correlated to the local density of geometrically necessary dislocations, the EBSD analyses carried out on the undeformed microstructures show traces of plastic deformation in the two phases but with differences in intensity and homogeneity. The origin of plastic deformation in the undeformed microstructure of the VAR and SSS composites may differ. In the VAR, the presence of dislocations in the Cu matrix of the undeformed microstructure was attributed to the difference in thermal expansion coefficients between the Cu matrix and the Cr reinforcing phase (Varoto et al., 2024). Given that the Cr phase is homogeneously distributed in the Cu matrix, it is not surprising that the KAM is also rather homogeneously distributed in this phase. In the SSS composite, the presence of interfacial pores significantly restricts the formation of GNDs at the interface due to thermal mismatch. Interestingly, the regions of the Cu matrix that are highly disoriented in the SSS composite correspond to confined areas between Cr particles. This may be due to residual local plastic deformation of the Cu matrix during compression of the green body that was not fully eliminated during sintering. In our previous work (Varoto et al., 2024), the large disorientation observed locally in the Cr phase of the VAR composite was attributed to the elastic anisotropy of the Cu and Cr crystals, which create heterogeneous strain fields that are locally accommodated by plastic deformation.

3.2. *Mechanical response and deformed microstructures*

The true stress - true strain tensile response of both SSS and VAR are given in Fig. 3a and b where the results of the monotonic and interrupted tensile tests are superimposed. The yield strength taken at 0.2% plastic strain of the SSS material (105 MPa) is half the one of its VAR counterpart (200 MPa). The ultimate tensile strength reaches nearly 400 MPa in the VAR and only 270 MPa in the SSS.

The ROIs selected in the VAR and SSS samples, i.e., the regions highlighted with dashed yellow lines in Fig. 1b and c, were then systematically characterized by EBSD after different increments of tensile strain. Fig. 4 shows the evolutions of the KAM in the Cu matrix and Cr reinforcement upon straining in both composites. These maps show that the KAM increases with tensile straining in the Cu matrix of both composites. In the VAR composite, deformation appears self-similar: the regions with the highest KAM do not evolve, but rather, the intensity of KAM in these regions increases. In the SSS composite, an increase in KAM is observed near the pores located in the Cu matrix. Conversely, there is almost no evolution of the KAM in the Cr reinforcing phase. The KAM evolution upon straining can be analyzed more quantitatively by

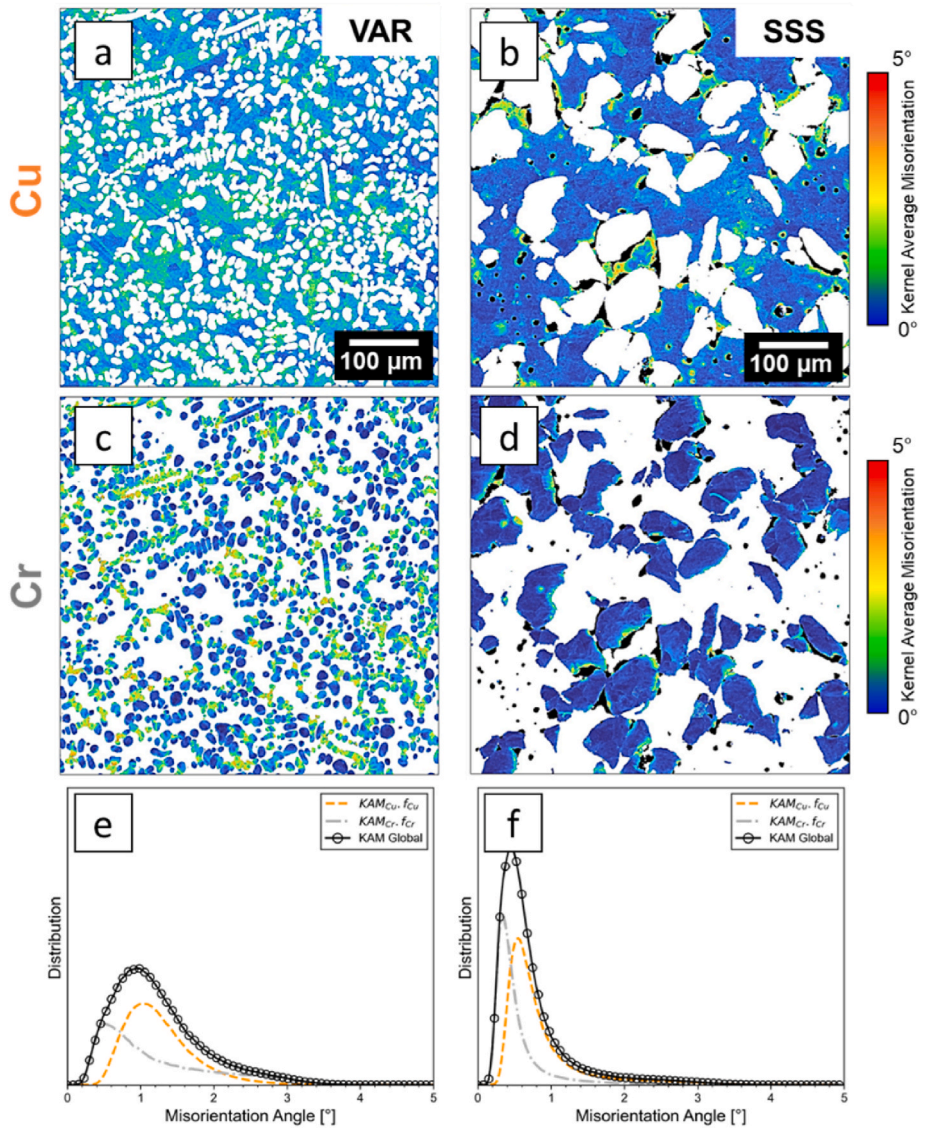


Fig. 2. KAM maps in the Cu (a,b) and Cr (c,d) phase in the undeformed microstructures of the Cu-35Cr composite produced by VAR and SSS respectively. Normalized distributions of the KAM in the entire ROI and in each phase in the VAR (e), and SSS (f) microstructure. The distributions have been normalized by the respective volume fraction of each phase.

plotting the KAM distributions in both phases after different tensile strain increments (see Fig. 5a for the VAR and Fig. 5b for the SSS composite). Upon straining, the KAM distributions are shifted towards larger disorientations in the Cu phase and this trend is observed in the two composites. The increase in plastic strain in the Cu phase is reflected by the evolution of the average KAM in the Cu phase as a function of tensile strain, see Fig. 5c. On the opposite, the average KAM in the Cr phase (Fig. 5d) remains nearly unchanged up to 4% tensile strain but increased slightly at 6% tensile strain, suggesting that during the first stages of deformation, the Cr phase is mostly elastically loaded.

4. Effect of various microstructural features on the tensile response using crystal plasticity simulations

In this section, we first describe the simulation framework and then validate the model based on the Cu-35Cr VAR composite. The idea is to keep the model as simple as possible by reducing the number of adjustable parameters in the crystal plasticity model. The model is then used to study the influence of different microstructural features on the mechanical response of the Cu-35Cr SSS composite.

4.1. Simulation framework

The EBSD maps collected at the center of the gauge length of the undeformed tensile specimens were used as input for the 2D crystal plasticity calculations (areas highlighted with yellow dashed lines in Fig. 1b and c). In the ROI of the VAR sample, the relative area fraction of the Cu and Cr phase was respectively found equal to 56 and 44% respectively. In the ROI of the SSS sample, Cu represents also 56% but the area fraction of the Cr phase is 41%, the remaining 3% corresponds to the porosity (matrix and interfacial pores). The FFT grid size in the simulations is 1024×1024 pixels. Each pixel is being assigned a set of initial Euler angles from the EBSD maps, meaning that initial local disorientations within grains are included in the simulations. Each voxel is then assigned a phase number, which can be 1 (Cu), 2 (Cr), 3 (matrix pores), or 4 (interfacial pores). When modeling the sintered microstructure, we open the possibility to virtually fill matrix pores and/or interfacial pores with Cu or Cr, to quantify the effect of pores on the mechanical response. EVP-FFT simulations are performed to simulate uniaxial tension by imposing a macroscopic strain-rate of $0.001s^{-1}$ along the same direction as in the experiments. In the transverse

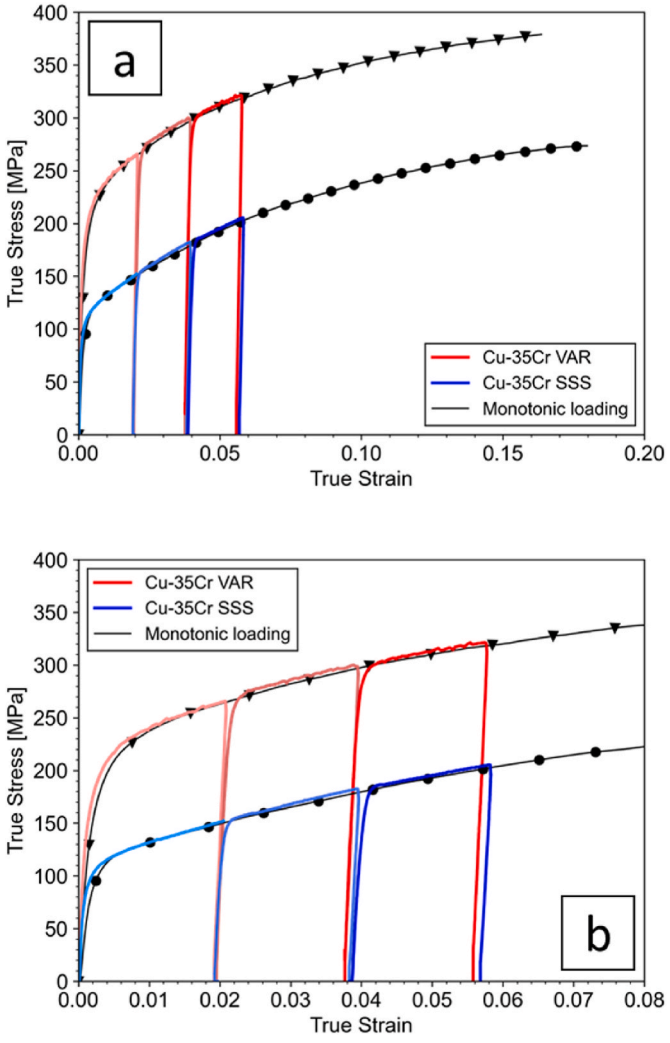


Fig. 3. True stress-strain curves of the Cu-35Cr processed by VAR and SSS: (a) overview of the tensile responses and (b) enlarged view between 0 and 8% tensile strain. Note that both monotonic and interrupted tensile tests are displayed.

directions to the tensile axis (TD and ND), the macroscopic normal stresses are imposed to be zero. All macroscopic shear distortions are imposed to be zero. In simulations, the total macroscopic tensile strain was limited to 6%, and we use a small-strain formulation (still accounting for lattice rotations (Lebensohn et al., 2012)) because the experimental microstructure does not show significant morphological changes in this range of strains. We establish comparisons between simulation results and experimental data at tensile strains of 2, 4, and 6%. Comparisons include macroscopic stress-strain curves and KAM maps and distributions. In the simulations, the stress-strain curves correspond to the evolution of the normal stress in the tensile direction as a function of the mean normal strain in the same direction. We note that our FFT simulations assume periodic boundary conditions. In the present simulations, we did not apply any particular treatment at edges. Because of the large size of the ROIs that contain a large number of phases and grains (strongly spatially heterogeneous microstructure), and because of the large number of voxels (and thus of Fourier frequencies) in each direction, we do not observe any significant effect of periodic boundary conditions at the edges (which can be checked by looking at different mechanical fields shown in the figures in the supplementary materials). Furthermore, the central part of the simulated volumes (excluding the edges) contains sufficient microstructural heterogeneities to be statistically representative of the materials studied.

For modeling plastic strain evolution and strain hardening in the Cu phase, we use a crystal plasticity model, considering the 12 FCC {111}< 110> slip systems (Lebensohn and Needleman, 2016; Tome et al., 1984; Patil et al., 2021). For a given resolved shear stress on the slip system s, τ^s, the flow rule relating the associated plastic shear rate follows the power law (Hutchinson, 1977):

$$\dot{\gamma}^s = \dot{\gamma}_0 \left| \frac{\tau^s}{\tau_c^s} \right|^{\frac{1}{m}} sign(\tau^s), \tag{1}$$

where $\dot{\gamma}_0$ is a reference plastic shear rate and m is the rate sensitivity of slip. For this alloy, a complex hardening law (e.g., a power or exponential law) requiring the calibration of multiple parameters proved unnecessary. Instead, a simple isotropic linear hardening law was adopted, as it allows for an accurate fit of the mechanical response of the VAR and SSS composites without introducing an excessive number of parameters. Therefore, the evolution of the critical resolved shear stress (CRSS) τ_c^s on slip system s is expressed as:

$$\tau_c^s = \tau_0^s + \theta_0^s \Gamma. \tag{2}$$

In the above equation, τ_0^s and θ_0^s denote the initial CRSS and hardening rate, respectively. They are taken the same for all slip systems. Γ denotes the plastic slip accumulated over all the slip systems. Firstly, θ_0^s in the Cu phase was calibrated and kept constant in all the simulations regardless of the material considered, VAR or SSS. Because the yield stress of chromium is assumed to be large (see below), the value of τ_0^s in the Cu phase needs to be calibrated in order to fit the macroscopic yield stress in the experimental stress-strain curves. The only difference between the VAR and SSS is a larger τ_0^s in the VAR (52 vs. 35 MPa). The difference in τ_0^s in the Cu matrix between the VAR and the SSS composites can have two origins: (i) a difference in dislocation density; and (ii) a difference in grain size. However, with a grain size of 15 μm in the VAR and 25 μm in the SSS, it is reasonable to neglect the impact of grain size on τ_0^s. Indeed, grain boundary strengthening through a Hall-Petch effect is limited in this range of grain size, see (Hansen, 2004; Miura et al., 2009). Thus, we consider that the difference in τ_0^s between the VAR and SSS composites results mainly from a difference in dislocation density. This is in line with the KAM measurements carried out in the as-received material (Fig. 2) which show that the average disorientation in the Cu matrix of the VAR is twice as large than in the matrix of the SSS. The model parameters used for copper are summarized in Table 1. Elastic stiffness coefficients are taken from (Chang et al., 2010).

For the chromium phase, we use the same constitutive equations. We consider the 12 BCC {110}<111> slip systems. Cr is assumed to be elastic – perfectly plastic ($\theta_0^s = 0$), with a large and constant lattice friction $\tau_0^s = 200$ MPa. This single parameter enables to reproduce the tensile response of the VAR and SSS composites and is in relatively good agreement with literature data on Cr from (Marcinkowski and Lipsitt, 1962). Indeed, compression tests of polycrystalline Cr revealed that it follows the Hall-Petch law and lies in the range 200-370 MPa (at 273K) for grain sizes in the range 0.030-1 mm (Marcinkowski and Lipsitt, 1962). Material parameters used for Cr in the simulations are also given in Table 1. Elastic stiffness coefficients are taken from (Bolef and De Klerk, 1963). Note that including non-Schmid behavior would be more appropriate than the simple power law used here, see e.g. (Bienvenu et al., 2022; Bienvenu and Clouet, 2022). In the present study, however, the two Cu-35Cr composite materials investigated (VAR and SSS) show negligible plastic deformation in the Cr phase, as revealed by the experimental KAMs measured between 0 and 6% tensile strain. As such, for the materials and the strain range considered, we are convinced that a simple power law with a large friction stress is a reasonable choice. We also would like to remind that the objective was to use as few material parameters as possible in our CPFFT model to probe microstructural effects on the mechanical response.

The pores in the sintered microstructure are modeled as a gas phase

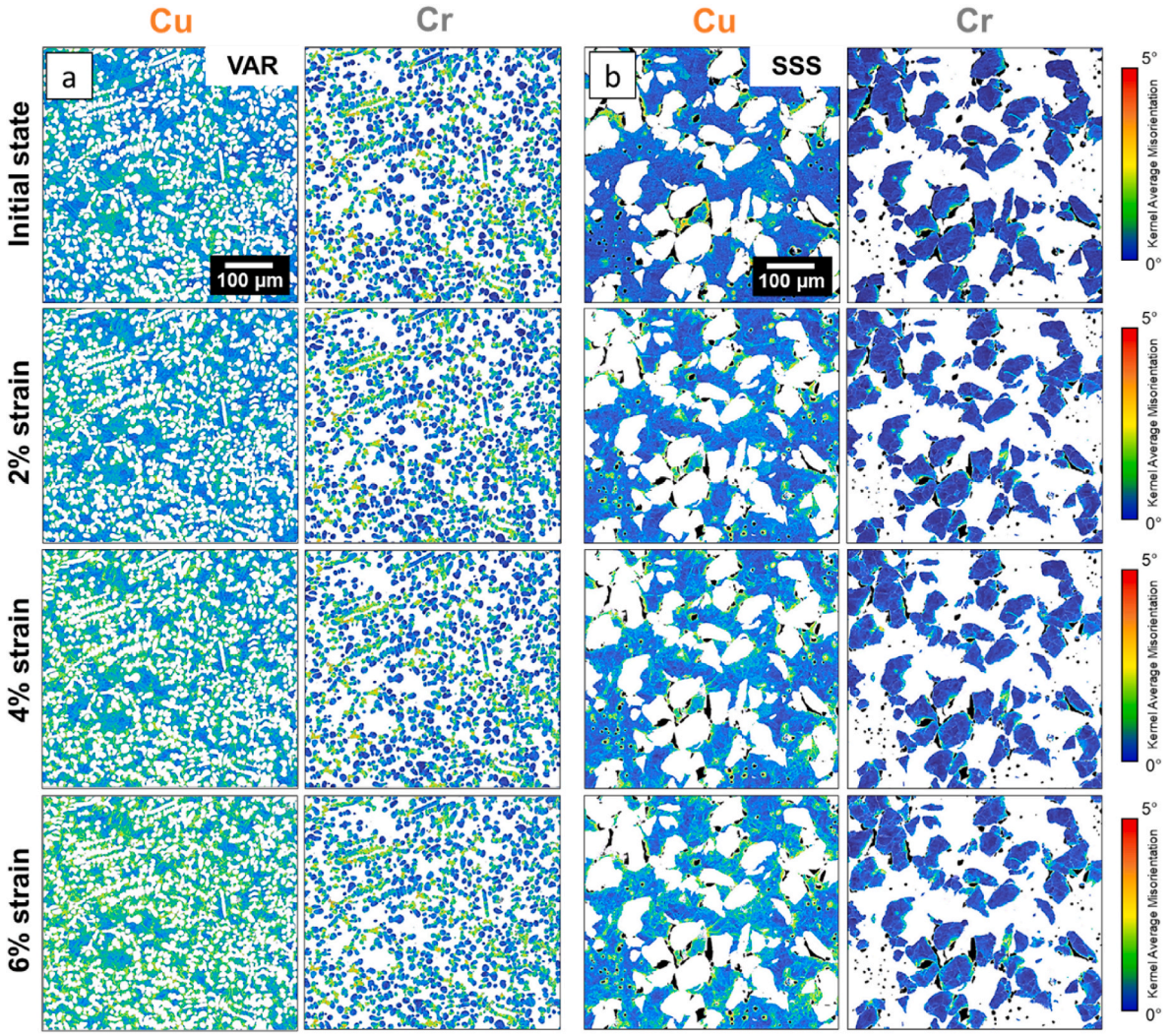


Fig. 4. Evolutions of the KAM maps upon straining (undeformed, 2%, 4% and 6% of tensile strain) in the Cu and Cr phase in (a) the VAR and (b) in the SSS.

(i.e. elastic phase with a negligible elastic stiffness), which allows having null stresses inside pores and satisfying zero-tension at the pore surfaces. As aforementioned, the simulation predictions will be compared to experiments in terms of macroscopic tensile response and local KAM distributions. As such, within the course of plastic deformation, the local initial Euler angles are updated with the local values of the elastic rotation. The simulation code then generates post-processing data files that can be analyzed with the MTEX toolkit to plot KAM maps, which can then be compared with the experimental ones.

While the present model used here is phenomenological, comparisons can be made with dislocation density-based models, such as the Kocks-Mecking model (Chang et al., 2010; Kocks and Mecking, 2003; Tabourot et al., 1997). Based on a recent work (Patil et al., 2021), the value of the initial CRSS τ_0^s can be converted into an equivalent dislocation density. The total dislocation density (sum over the N slip systems) in copper is (Patil et al., 2021):

$$\rho_{tot} = \left(\frac{\sum_{s=1}^{N} \tau_0^s}{N\alpha\mu b} \right)^2 = \left(\frac{\tau_0^s}{\alpha\mu b} \right)^2, \quad (4)$$

where N = 12, α = 0.5, $\mu = \sqrt{0.5C_{44}(C_{11}\text{-}C_{12})}$ = 42 GPa, and b = 0.256 nm. The initial CRSS of copper adjusted to fit the experimental stress-strain curves for VAR (τ_0^s = 52 MPa) and SSS (τ_0^s = 35 MPa) materials is equivalent to total dislocation densities of 9.3×10^{13} m^{-2} (7.8×10^{12} m^{-2} per slip system) for the VAR composite and 4.2×10^{13} m^{-2} (3.5×10^{12} m^{-2} per slip system) for the SSS material. Although these magnitudes cannot be quantitatively compared with experimental measures in this work, we predict a ratio of nearly 2 between the initial dislocation densities in the Cu phase in the VAR and SSS, which is on the order of that between initial average disorientations in Cu in VAR and SSS materials measured by EBSD.

4.2. Validation on the VAR

The crystal plasticity simulations were first validated based on the Cu-35Cr VAR microstructure because it is fully dense and thus it allows neglecting the effect of matrix and interfacial pores on the mechanical response. Only three parameters were adjusted to reproduce the experimental stress-strain curve: the initial CRSS τ_0^s in both Cu and Cr, and θ_0^s in the Cu phase. The values that best fit the experimental data of the VAR composite are shown in Table 1. The tensile response of the Cu-35Cr VAR composite (pink circle symbols) shows a very good agreement with the experimental stress-strain response (black dashed curve), see Fig. 6.

The evolution of the local disorientation distribution extracted from the simulations has been also compared with the experimental data. We note that because initial Euler angles from EBSD orientation maps are used as input for every voxel in the CPFFT simulations, the initial

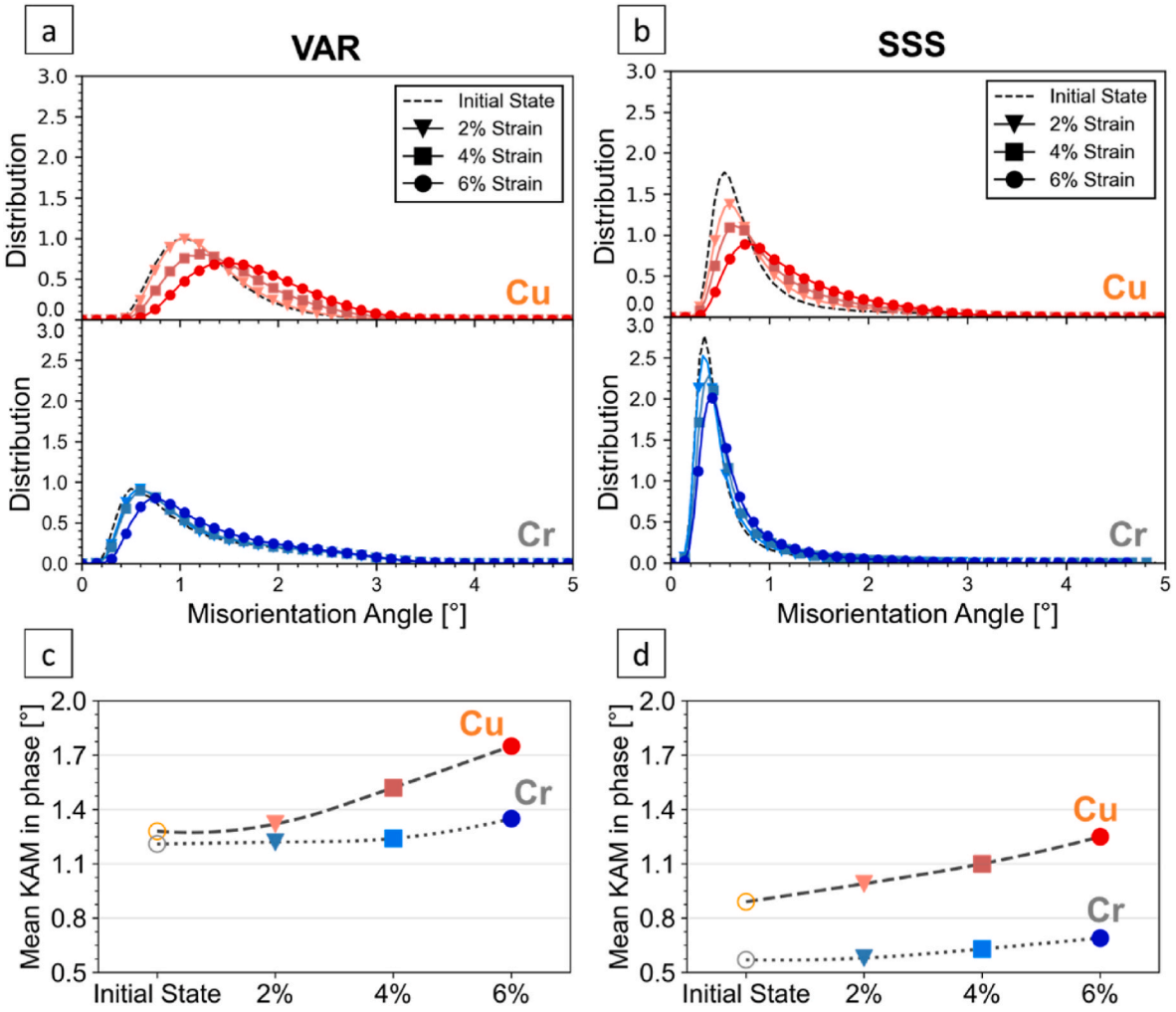


Fig. 5. Evolution of the local disorientation distributions upon straining in the Cu and Cr phase: (a) in the VAR and (b) in the SSS. Evolution of the average KAM in the Cu and Cr phase as a function of the macroscopic tensile strain: (c) in the VAR and (d) in the SSS.

Table 1
Parameters used in the simulations for the Cu and Cr phase.

	C_{11} (GPa)	C_{12} (GPa)	C_{44} (GPa)	$\dot{\gamma}_0$ (s^{-1})	m	τ_0^s (MPa)	θ_0^s (MPa)
Cu phase	168.4	121.4	75.4	0.001	0.05	52 (VAR) 35 (SSS)	100
Cr phase	392	91	103	0.001	0.05	200 (VAR) 200 (SSS)	0

experimental KAM maps (see Fig. 4) and the simulated ones are the same, and they only differ with deformation. The experimental and simulated KAM maps in the Cu matrix after 6% strain are compared in Fig. 7a and b, respectively. In the Cu phase, there is a larger fraction of highly disoriented regions in the FFT simulation suggesting that we are more sensitive to strain amplification in the 2D FFT calculations. Comparisons between the experimental KAM distributions in the Cu and the simulated ones after 2%, 4% and 6% tensile strain are shown in Fig. 8a. The KAM distributions in the Cu phase from the simulations are all shifted towards slightly larger disorientations in comparison with the experimental KAM distributions regardless of the tensile strain applied. The peak value is shifted by approximately 1°, and the standard deviation is also slightly larger, characteristic of a more heterogeneous KAM field. These discrepancies might originate from the 2D nature of our simulations, which does not take into account the out-of-plane plastic activity and can predict more heterogeneous deformation fields than 3D simulations (Roters et al., 2019; Mirhosseini et al., 2023; Diehl et al., 2017; Xia et al., 2025). This 2D artefact might be reinforced because in the condition of 2D plane strain, the Cr phase (almost purely elastic), and the pores in the case of the SSS material, are infinitely extruded in the thickness direction. The discrepancies in KAM maps might also be due to the absence of kinematic hardening in the model, which should partially recover plastic strains during the unloading stages and thus reduce the local intensity in the KAM maps. 3D simulations based on X-ray tomography data (Varoto et al., 2023), and accounting for kinematic hardening (Lebensohn and Needleman, 2016), will be performed in a forthcoming study to tackle these points more specifically but are beyond the scope of the present work.

In the Cr phase, the simulated KAM distribution shows a very good agreement with the experimental data (Fig. 8b). The Cr phase remains mostly elastically loaded after 4% tensile strain and first signs of plastic deformation are only detected after 6% strain as illustrated by the slight

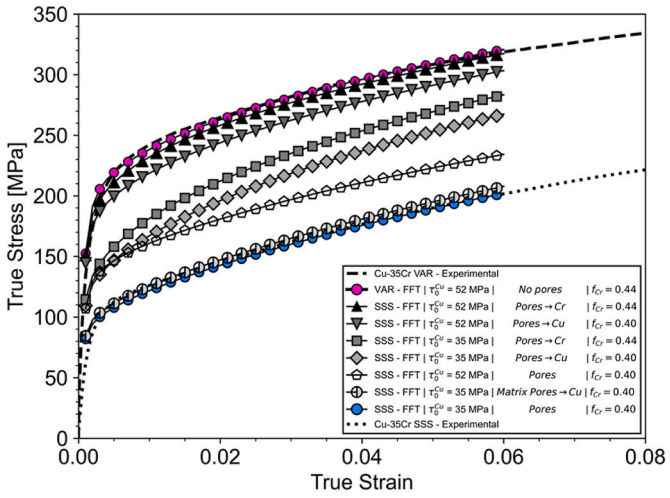


Fig. 6. Comparison of the experimental tensile response of the VAR and SSS composites with the results from the different simulations conducted.

shift of the KAM distribution towards larger disorientation at 6% tensile strain.

To further validate the full-field approach employed in this study, we evaluate the ability of the model to capture the spatial distribution of local disorientation heterogeneities revealed in the KAM maps. To circumvent the higher strain amplification observed in the simulations, the KAM maps determined experimentally and the ones derived from the crystal plasticity simulations have been normalized as follows. We first computed the average KAM in each phase ($<KAM>_{Cu}$ and $<KAM>_{Cr}$) over the entire ROI. Then, the local KAM at every pixel i in the map was normalized by dividing it by the average $<KAM>_{Cu,Cr}$ per phase (normalized KAM $= KAM_i/<KAM>_{Cu,Cr}$). This artificial normalization is solely introduced to check whether or not the KAM maps predicted by the simulations agree qualitatively well, spatially, with the experimental ones. In addition to retrieving the macroscopic stress-strain curves, we also impose that the validated model should predict spatial field distributions that agree qualitatively well (despite it is 2D) with experimental fields. The normalized experimental and simulated KAM maps in the Cu phase were then generated and compared, see Fig. 7c and d, respectively. The normalized KAM maps from the experiments and simulations show a very good agreement. For example, the regions with low KAM are spatially distributed in the same areas. Interestingly, by normalizing the KAM, the difference between the experiments and the simulations in the Cu matrix has been significantly decreased, see Fig. 8c. This suggests that the larger strain amplification observed in the raw KAM distribution in the Cu phase results mainly from the limitations of the model. A similar comparison was established for the Cr phase, the results can be found in Figure S 1 and Fig. 8b and d. For the Cr phase, we found consistent results regardless of looking at the raw data or the normalized data. This shows that the Cr phase is not subjected to strain amplification as the softer Cu phase, most likely because the plastic deformation in the Cr phase is limited until 4% tensile strain.

4.3. Validation on the SSS: effect of the initial dislocation density

We ran a first simulation to model the tensile response of the SSS composite taking into account the presence of pores and using the parameters of the Cu phase that allows us to reproduce the tensile response of the VAR composite. The result is shown in Fig. 6, see the curve with unfilled pentagonal symbols. In this simulation, the SSS composite yields at a larger stress than in the experiment. This is not surprising as we used for the Cu phase the parameters that were calibrated for the VAR composite ($\tau_0^s = 52$ MPa, $\theta_0^s = 100$ MPa). Experimentally, we did observe from the KAM maps collected in the undeformed microstructures that the average disorientation in the Cu phase was twice lower in the SSS than in the VAR material (see Fig. 5). This suggests that the initial GND

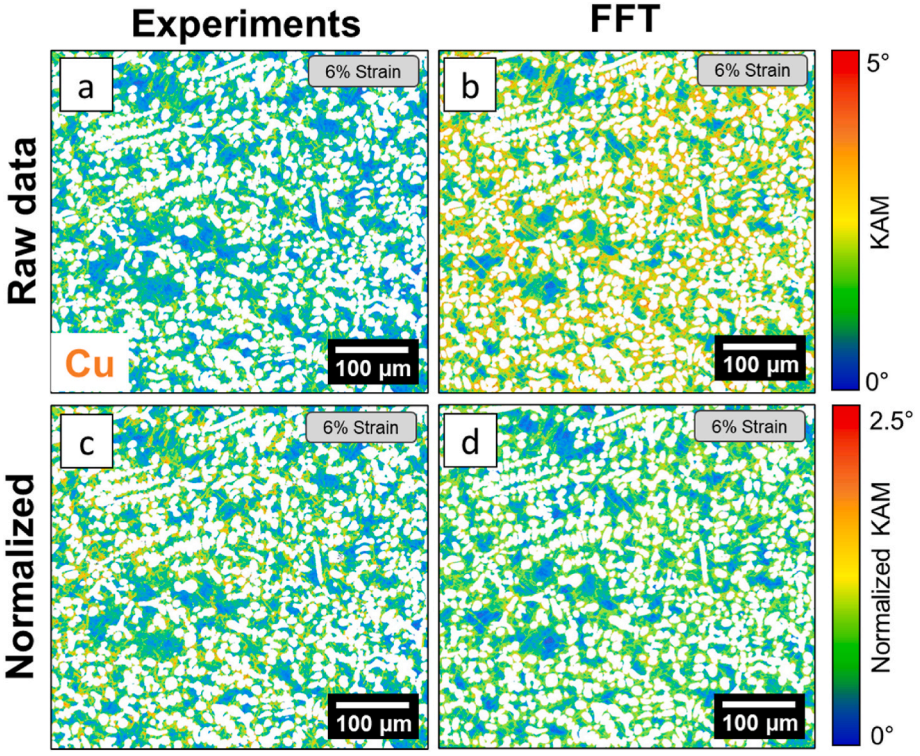


Fig. 7. Comparison of the KAM maps in the Cu phase after 6% tensile strain in the VAR composite: (a) experiment (raw data) and (b) crystal plasticity simulation (raw data). Comparison of the normalized KAM ($KAM_{Cu}/<KAM>_{Cu}$) distributions after 6% tensile strain in the VAR composite: (c) experiment and (d) crystal plasticity simulations.

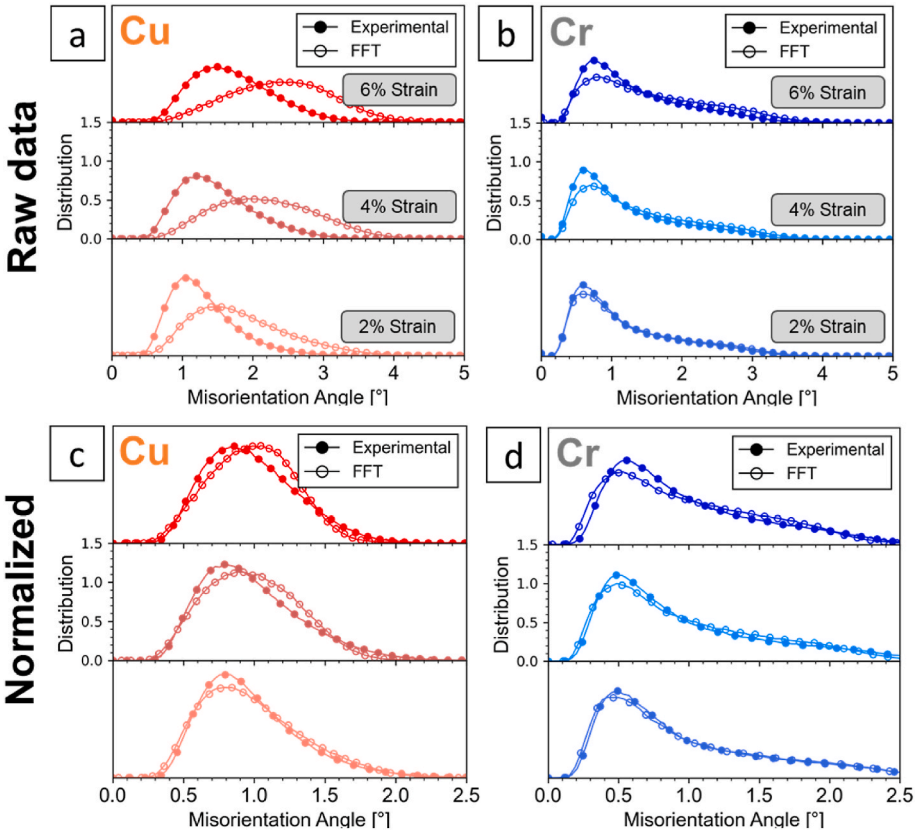


Fig. 8. (a) KAM distributions (a) in the Cu phase and (b) in the Cr phase of the VAR composite. (c) Normalized KAM distributions (c) in the Cu phase and (d) in the Cr phase of the VAR composite.

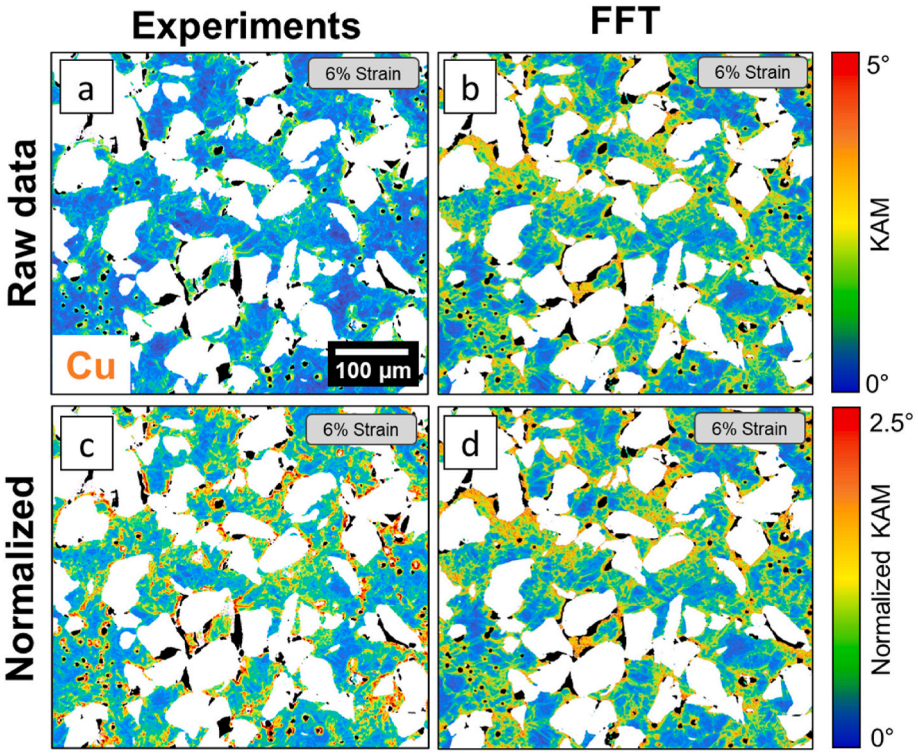


Fig. 9. Comparison of the KAM maps in the Cu phase after 6% tensile strain in the SSS composite: (a) experiment (raw data) and (b) crystal plasticity simulation (raw data). Comparison of the normalized KAM ($KAM_{Cu}/<KAM>_{Cu}$) distributions after 6% tensile strain in the SSS composite: (c) experiment and (d) crystal plasticity simulations.

density in the Cu phase is lower in the SSS composite than in its VAR counterpart. Consequently, we run an additional simulation of the tensile response of the SSS composite by only decreasing τ_0^s (taken equal to 35 MPa instead of 52 MPa) while θ_0^s was kept constant. Decreasing τ_0^s is equivalent to decrease the initial dislocation density in the Cu phase as highlighted earlier in this manuscript, see equation (4). The simulated tensile response of the SSS composite taking now for the Cu phase $\tau_0^s =$ 35 MPa corresponds to the curve with blue circles in Fig. 6. Now, the simulated tensile response matches very well the one determined experimentally for the SSS composite (Fig. 6) while all the other parameters were kept unchanged.

As in the VAR composite, the comparison of the evolution of the KAM maps determined experimentally (Fig. 9a) with the ones calculated from the crystal plasticity simulations (Fig. 9b) shows that the model results in a larger strain amplification in the Cu phase. After normalization of the KAM, a very good agreement is found between the experiments and the model, see comparison between Fig. 9c and d. More quantitative comparisons between the experiments and the simulations have also been established by looking at the KAM distributions. The simulations tend to overestimate the disorientation in the Cu phase regardless of the tensile strain (Fig. 10a). In the Cr phase, a good agreement is again found: the KAM distributions in the Cr phase are nearly superimposed, see Fig. 10b and the KAM maps in the Cr phase are similar (Figure S 2). Normalizing the KAM allows to verify that the model captures well the spatial heterogeneity in disorientation in the Cu phase (Fig. 10c).

4.4. Effect of porosity

Once the full-field model was calibrated and validated on the VAR and SSS composites, the effect of porosity on the tensile response of the Cu-Cr composite can now be investigated by artificially filling the pores to make the SSS composite fully dense. If only one pore population is filled in, it becomes possible to discriminate the effect of matrix pores from the effect of interfacial pores.

First, the matrix pores of the SSS composite were filled with Cu (no change in area fraction of Cr, $f_{Cr} = 40\%$). This simulation corresponds to the curve with the half-filled circle symbols in Fig. 6. The curve nearly overlaps that of the SSS composite taking into account all pores (matrix and interfacial pores). This shows that the matrix pores have a negligible effect on the tensile response of the SSS composite. All pores, i.e., both matrix and interfacial, were then filled with Cu making the material fully dense (no change in area fraction of Cr, $f_{Cr} = 40\%$). The associated tensile response is plotted using gray diamond symbols in Fig. 6. The tensile response of such a composite is now well above that of the SSS composite (curve with blue circles in Fig. 6). This shows that the interfacial pores play a significant role in the tensile response of the SSS composite.

Finally, all the pores were filled with Cu but we took the same $\tau_0^s =$ 52 MPa as the one allowing to reproduce the VAR tensile response. This allows us to evaluate the combined effect of the suppression of pores and the increase of the initial dislocation density in the Cu matrix. We recall here that the area fraction of Cr is unchanged ($f_{Cr} = 40\%$) since pores were filled with Cu. The simulated tensile response is given in Fig. 6 using the inversed gray triangles. Now the tensile response of such a fully dense SSS composite gets closer but still remains below the tensile response of the VAR composite. At this stage, the discrepancy between the tensile response of the VAR composite with the simulated one of the SSS with pores filled with Cu and the same dislocation density as in the VAR are still unclear. Two factors can be invoked to explain these discrepancies: (i) the fraction of Cr, $f_{Cr} = 44\%$ in the VAR and $f_{Cr} = 40\%$ in the SSS when pores are filled with Cu, and (ii) the change in morphology of the Cr phase (equiaxed in the SSS and dendritic in the VAR).

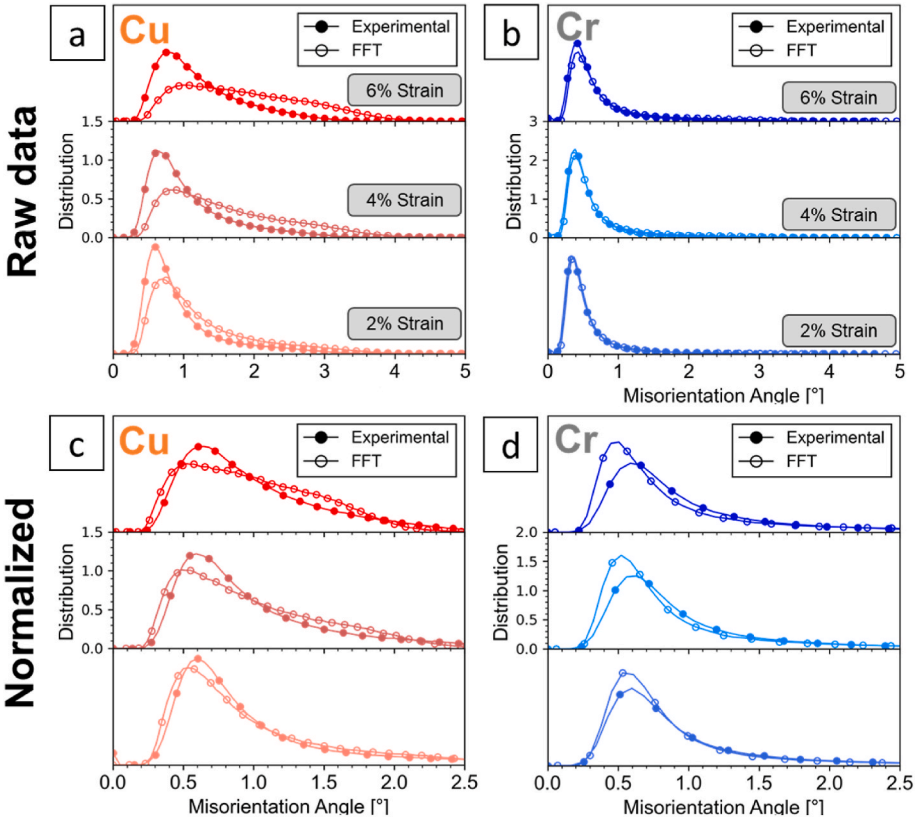


Fig. 10. (a) KAM distributions (a) in the Cu phase and (b) in the Cr phase of the SSS composite. (c) Normalized KAM distributions (c) in the Cu phase and (d) in the Cr phase of the SSS composite.

4.5. Impact of the Cr volume fraction and morphology

Another simulation was conducted with the pores filled with Cr instead of Cu while taking $\tau_0^s = 52$ MPa to maintain the same initial dislocation density as in the VAR. Interestingly, filling the pores of the SSS composite with Cr gives a Cr fraction of 44%, which is similar to that of the VAR. The simulated tensile response of the SSS composite with Cr-filled pores corresponds to the curve with filled black triangles in Fig. 6. Increasing the Cr area fraction from 40% to 44% (a relative increase of about 10%) shifts the tensile response of the SSS composite towards larger stresses, bringing it now very close to that of the VAR. This simulation highlights the key role played by the volume fraction of Cr in these Cu-Cr composites. Conversely, since the main difference between the SSS composite with pores filled with Cr and its VAR counterpart is in the morphology of the Cr phase, and since the tensile responses are very similar, this suggests that the Cr phase morphology does not significantly affect the tensile response of such composites.

4.6. Stress partitioning in Cu-35Cr composites

The outputs from the full-field crystal plasticity simulations can be exploited to investigate stress partitioning in the Cu-35Cr composites. The tensile stress fields of both VAR and SSS composites after different increments of strain can be found in supplementary materials, see Figure S 3 and Figure S 4, respectively. Microstructural changes that have the strongest influence on stress partitioning between the soft Cu matrix and the harder Cr-reinforcements can be identified. The tensile stress distribution within the Cu and Cr phase in different Cu-35Cr composites after 6% tensile strain are given in Fig. 11a and b, respectively. The increase of the initial dislocation density through the increase from $\tau_0^s = 35$ MPa to 52 MPa slightly shifts the tensile stress distribution in the Cu and Cr phases towards large stresses. However, the most pronounced effect on the tensile stress distribution in both phases is observed when interfacial pores are filled, significantly shifting the distribution toward higher stress levels.

These tensile stress distributions were further analyzed by calculating (i) the standard deviation that gives hints regarding the tensile stress heterogeneity in each phase (Fig. 12a and b), and (ii) the mean tensile stress in each phase (Fig. 12c and d). Interestingly, the different microstructural changes do not seem to significantly affect the heterogeneity in tensile stress within the Cu matrix. An increase of the initial dislocation density in the Cu phase (increase in τ_0^s in the Cu matrix) slightly increases the stress heterogeneities in the Cu phase while filling pores with Cu results in a more homogeneous stress field (Fig. 12a). The effect of filling matrix and interfacial pores with Cu on the heterogeneity in tensile stress in the Cr phase is remarkable as it significantly decreases the standard deviation (Fig. 12b). In other words, filling pores with Cu makes the stress more homogeneous. The analysis of the evolution of the mean tensile stress in the Cu phase after 6% tensile strain reveals that the two microstructural features having the greatest impact are the increase of the initial dislocation density in the Cu phase and the filling of all pores with Cu, see Fig. 12c. The effect of the initial dislocation density in the Cu phase on the mean tensile stress after 6% tensile strain appears limited in the Cr phase. However, it is worth highlighting that filling pores (especially interfacial pores with Cu) results in a significant increase in mean tensile stress in the Cr phase. This shows that the load transfer from the Cu matrix to the Cr particles becomes more efficient upon straining when interfacial pores are filled.

We shall finally remind that our 2D simulations assume plane strain conditions. This can result in significant out-of-plane shear stresses. Also, the Cr phase (almost purely elastic), and the pores in the case of the SSS material, are assumed to be infinitely extruded in the thickness direction. As such, the prediction of stresses inside phases are necessarily affected by the 2D nature of our simulations. As aforementioned, 3D simulations based on X-ray tomography data (Varoto et al., 2023), will be performed in a forthcoming study, which will allow comparing 2D versus 3D effects on the distribution of stresses in phases.

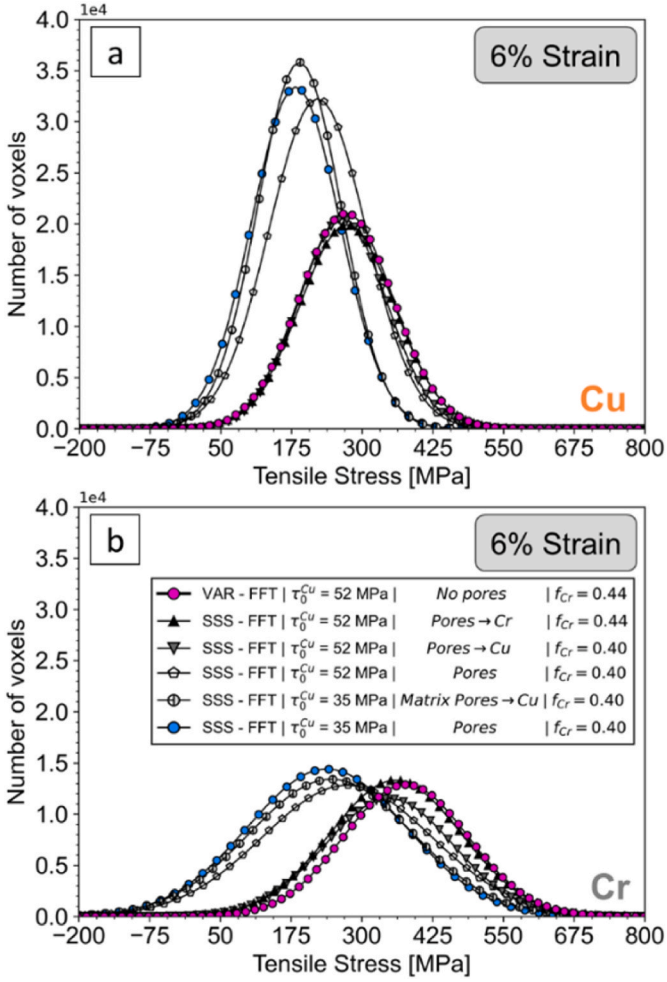


Fig. 11. Tensile stress distributions extracted from the crystal plasticity simulations after 6% tensile strain in different Cu-35Cr composites: (a) in the Cu and (b) in the Cr phase.

5. Summary and conclusion

The microstructural features affecting the tensile response of Cu-35Cr composites were investigated using full-field crystal-plasticity simulations and a simple linear hardening law in each phase. The aim was to distinguish the impact of various parameters, including the initial dislocation density in the Cu matrix, pores (in the matrix or at the interface), morphology of the Cr phase, and minor variations in the volume fraction of the two phases. It is worth noting that it would not have been possible to discriminate the effect of these features experimentally. This motivated the use of a modelling approach. The full-field crystal-plasticity model was first calibrated and validated based on experiments. Two Cu-35Cr composites, fabricated using two different processes (casting for the VAR and sintering for the SSS), were investigated. The latter contains matrix and interface porosity. Their tensile response was determined using monotonic and interrupted tensile tests, the latter coupled with EBSD measurements conducted at different strain increments. We note that the use of a full field model is fully justified in the present study. Not only does the model capture the experimental tensile responses of the VAR and SSS materials, but it is further validated by providing a good representation of the spatial distribution of local disorientation heterogeneities. The validated model can then be used to monitor the local elastoplastic deformation and

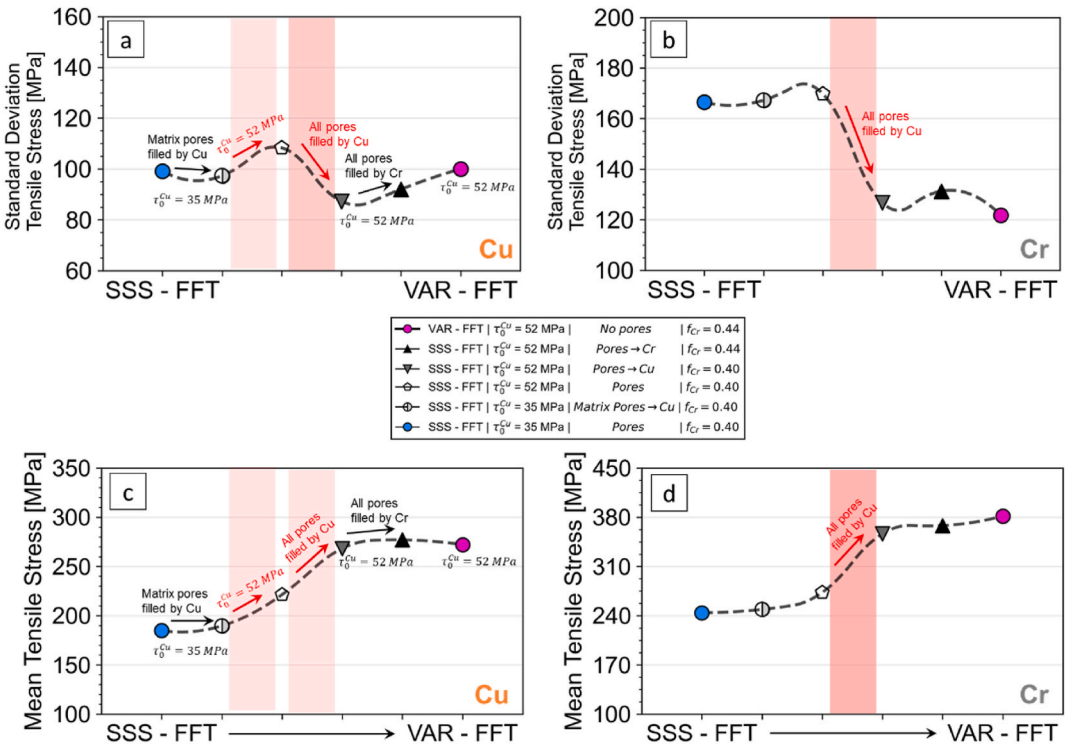


Fig. 12. Standard deviation of the tensile stress distributions of the different Cu-35Cr composites after 6% tensile strain: (a) in the Cu phase and (b) in the Cr phase. Mean tensile stress computed from the stress distributions extracted from the crystal plasticity simulations in different Cu-35Cr composites: (c) in the Cu and (d) in the Cr phase. Areas in red highlight the most significant variations.

hardening in both Cu and Cr phases, quantify the load transfer from Cu to Cr, and the resulting macroscopic strain hardening. The model finally allows differentiating the effect of interfacial pores from that of matrix pores. The conclusions from this work can be summarized as follows:

- Pores in the Cu matrix with a nearly spherical morphology, representing only 10% of the overall porosity, have a negligible effect on the tensile response of Cu-35Cr composites.
- The morphology of the Cr phase does not appear to significantly influence the tensile response of Cu-35Cr composites. The tensile response of SSS materials containing equiaxed Cr particles and Cr-filled pores (with the same Cr fraction as in the VAR) is superimposed to that of the VAR, which exhibits dendritic Cr.
- Small variations in the Cr fraction can slightly alter the tensile response of Cu-35Cr composites when all pores are filled.
- The initial dislocation density in the Cu matrix and the interfacial pores (which account for 90% of the overall porosity) play a significant role in the tensile response of Cu-35Cr composites. Dislocation density in the Cu matrix governs the yield point in the Cu phase, while interfacial pores limit load transfer to the reinforcing Cr phase.
- Filling the matrix and interfacial pores with copper mitigates stress heterogeneity at the microscale, particularly within the Cr phase.

CRediT authorship contribution statement

Lucas Varoto: Writing – original draft, Methodology, Investigation. **Guilhem Martin:** Writing – original draft, Methodology, Investigation. **Guillaume Hanon:** Writing – original draft, Methodology, Investigation. **Marc Fivel:** Writing – original draft, Methodology, Investigation. **Benoit Beausir:** Writing – original draft, Methodology, Investigation. **Ricardo A. Lebensohn:** Writing – original draft, Methodology, Investigation. **Vincent Taupin:** Writing – original draft, Methodology, Investigation.

Declaration of competing interest

The authors declare that they have no known competing financial interests or personal relationships that could have appeared to influence the work reported in this paper.

Acknowledgements

The Association Nationale de la Recherche Technologique (ANRT) are gratefully acknowledged for the financial support of this work through the grant CIFRE 2021/1619. VT, GM, MF and BB would like to acknowledge support from the French national research agency (ANR) through the Grant ANR-PRC-2024-IMP3D (ANR-24-CE08-3737). RAL acknowledges support from the Laboratory Directed Research and Development (LDRD) program at Los Alamos National Laboratory.

Appendix A. Supplementary data

Supplementary data to this article can be found online at https://doi.org/10.1016/j.mechmat.2026.105885.

Data availability

Data will be made available on request.

References

Bienvenu, B., Clouet, E., 2022. Ab initio modeling of slip activity in body-centered cubic chromium. Acta Mater. 224, 117485. https://doi.org/10.1016/j.actamat.2021.117485.

Bienvenu, B., Dezerald, L., Rodney, D., Clouet, E., 2022. Ab initio informed yield criterion across body-centered cubic transition metals. Acta Mater. 236, 118098. https://doi.org/10.1016/j.actamat.2022.118098.

Bolef, D.I., De Klerk, J., 1963. Anomalies in the elastic constants and thermal expansion of chromium single crystals. Phys. Rev. 129, 1063–1067. https://doi.org/10.1103/PhysRev.129.1063.

Chang, H.-J., Fivel, M., Rodney, D., Verdier, M., 2010. Multiscale modelling of indentation in FCC metals: from atomic to continuum, comptes rendus. Physique 11, 285–292. https://doi.org/10.1016/j.crhy.2010.07.007.

Diehl, M., An, D., Shanthraj, P., Zaefferer, S., Roters, F., Raabe, D., 2017. Crystal plasticity study on stress and strain partitioning in a measured 3D dual phase steel microstructure. Phys. Mesomech. 20, 311–323. https://doi.org/10.1134/S1029959917030079.

Ding, Bingjun, Yang, Zhimao, Wang, Xiaotian, 1996. Influence of microstructure on dielectric strength of CuCr contact materials in a vacuum. IEEE Trans. Compon. Packag. Manuf. Technol. A 19, 76–81. https://doi.org/10.1109/95.486565.

Genée, J., Berbenni, S., Gey, N., Lebensohn, R.A., Bonnet, F., 2020. Particle interspacing effects on the mechanical behavior of a Fe–TiB2 metal matrix composite using FFT-based mesoscopic field dislocation mechanics. Adv. Model. Simul. Eng. Sci. 7, 6. https://doi.org/10.1186/s40323-020-0141-z.

Han, J., Dou, Z., Zhang, T., An, W., 2023. Review of the recent Chinese research on the electrical properties of CuCr contacts for vacuum interrupters. J. Mater. Res. Technol. 25, 1585–1598. https://doi.org/10.1016/j.jmrt.2023.06.060.

Hansen, N., 2004. Hall–Petch relation and boundary strengthening. Scr. Mater. 51, 801–806. https://doi.org/10.1016/j.scriptamat.2004.06.002.

Hutchinson, J.W., 1977. Creep and plasticity of hexagonal polycrystals as related to single crystal slip. Metall. Trans. A 8, 1465–1469. https://doi.org/10.1007/BF02642860.

Jia, N., Roters, F., Eisenlohr, P., Raabe, D., Zhao, X., 2013. Simulation of shear banding in heterophase co-deformation: example of plane strain compressed Cu–Ag and Cu–Nb metal matrix composites. Acta Mater. 61, 4591–4606. https://doi.org/10.1016/j.actamat.2013.04.029.

Klinski-Wetzel, K.V., Kowanda, C., Heilmaier, M., Mueller, F.E.H., 2015. The influence of microstructural features on the electrical conductivity of solid phase sintered CuCr composites. J. Alloys Compd. 631, 237–247. https://doi.org/10.1016/j.jallcom.2014.12.249.

Kocks, U.F., Mecking, H., 2003. Physics and phenomenology of strain hardening: the FCC case. Prog. Mater. Sci. 48, 171–273. https://doi.org/10.1016/S0079-6425(02)00003-8.

Lebensohn, R.A., Kanjarla, A.K., Eisenlohr, P., 2012. An elasto-viscoplastic formulation based on fast fourier transforms for the prediction of micromechanical fields in polycrystalline materials. Int. J. Plast. 32–33, 59–69. https://doi.org/10.1016/j.ijplas.2011.12.005.

Lebensohn, R.A., Needleman, A., 2016. Numerical implementation of non-local polycrystal plasticity using fast fourier transforms. J. Mech. Phys. Solid. 97, 333–351. https://doi.org/10.1016/j.jmps.2016.03.023.

Marcinkowski, M.J., Lipsitt, H.A., 1962. The plastic deformation of chromium at low temperatures. Acta Metall. 10, 95–111. https://doi.org/10.1016/0001-6160(62)90055-X.

Mirhosseini, S., Perdahcıoğlu, E.S., Atzema, E.H., Van Den Boogaard, A.H., 2023. Response of 2D and 3D crystal plasticity models subjected to plane strain condition. Mech. Res. Commun. 128, 104047. https://doi.org/10.1016/j.mechrescom.2023.104047.

Miura, S., Ono, N., Nishimura, Y., 2009. Hall-Petch relation and twin boundaries in pure copper and Cu-Al alloys. J. Soc. Mater. Sci. Japan 58, 865–872. https://doi.org/10.2472/jsms.58.865.

Moulinec, H., Suquet, P., 1998. A numerical method for computing the overall response of nonlinear composites with complex microstructure. Comput. Methods Appl. Mech. Eng. 157, 69–94. https://doi.org/10.1016/S0045-7825(97)00218-1.

Papillon, A., Missiaen, J.-M., Chaix, J.-M., Roure, S., Schellekens, H., 2017. Sintering mechanisms of Cu-Cr metallic composites. Int. J. Refract. Metals Hard Mater. 65, 9–13. https://doi.org/10.1016/j.ijrmhm.2016.11.010.

Patil, C.S., Chakraborty, S., Niezgoda, S.R., 2021. Comparison of full field predictions of crystal plasticity simulations using the Voce and the dislocation density based hardening laws. Int. J. Plast. 147, 103099. https://doi.org/10.1016/j.ijplas.2021.103099.

Roters, F., Diehl, M., Shanthraj, P., Eisenlohr, P., Reuber, C., Wong, S.L., Maiti, T., Ebrahimi, A., Hochrainer, T., Fabritius, H.-O., Nikolov, S., Friák, M., Fujita, N., Grilli, N., Janssens, K.G.F., Jia, N., Kok, P.J.J., Ma, D., Meier, F., Werner, E., Stricker, M., Weygand, D., Raabe, D., 2019. DAMASK – the Düsseldorf advanced material simulation kit for modeling multi-physics crystal plasticity, thermal, and damage phenomena from the single crystal up to the component scale. Comput. Mater. Sci. 158, 420–478. https://doi.org/10.1016/j.commatsci.2018.04.030.

Slade, P.G., 2020. The Vacuum Interrupter: Theory, Design, and Application, second ed. CRC Press, Boca Raton.

Spaić, S., Komac, M., Fetahagić, A., 1989. Microstructure and properties of sintered Cu–25Cr alloy. Mater. Sci. Technol. 5, 1069–1073. https://doi.org/10.1179/mst.1989.5.11.1069.

Tabourot, L., Fivel, M., Rauch, E., 1997. Generalised constitutive laws for f.c.c. single crystals. Mater. Sci. Eng. A 234–236, 639–642. https://doi.org/10.1016/S0921-5093(97)00353-5.

Tome, C., Canova, G.R., Kocks, U.F., Christodoulou, N., Jonas, J.J., 1984. The relation between macroscopic and microscopic strain hardening in F.C.C. polycrystals. Acta Metall. 32, 1637–1653. https://doi.org/10.1016/0001-6160(84)90222-0.

Varoto, L., Blandin, J.-J., Lhuissier, P., Roure, S., Papillon, A., Chosson, M., Martin, G., 2023. 3D microstructure characterization of Cu 25Cr solid state sintered alloy using X-ray computed tomography and machine learning assisted segmentation. Mater. Charact. 203, 113107. https://doi.org/10.1016/j.matchar.2023.113107.

Varoto, L., Courtois, E., Nutor, R.K., Roure, S., Papillon, A., Chosson, M., Gault, B., Lhuissier, P., Blandin, J.-J., Martin, G., 2025. Microstructural features governing the effective thermal conductivity of Cu-25Cr sintered composites. Acta Mater. 301, 121601. https://doi.org/10.1016/j.actamat.2025.121601.

Varoto, L., Lhuissier, P., Blandin, J.-J., Roure, S., Papillon, A., Chosson, M., Martin, G., 2024. Influence of the processing route on the mechanical properties of Cu–35Cr metal matrix composites. Mater. Sci. Eng. A 908, 146953. https://doi.org/10.1016/j.msea.2024.146953.

Von Klinski-Wetzel, K., Kowanda, C., Boning, M., Heilmaier, M., Muller, F.E.H., 2012. Parameters influencing the electrical conductivity of CuCr alloys. In: 2012 25th International Symposium on Discharges and Electrical Insulation in Vacuum (ISDEIV). IEEE, Tomsk, Russia, pp. 392–395. https://doi.org/10.1109/DEIV.2012.6412536.

Xia, D., Li, Y., Qin, S., 2025. Out-of-plane constraint for 2D representative volume element model of dual phase steels under uniaxial tension. Comput. Mater. Sci. 246, 113490. https://doi.org/10.1016/j.commatsci.2024.113490.

Zecevic, M., Lebensohn, R.A., Capolungo, L., 2023. Non-local large-strain FFT-based formulation and its application to interface-dominated plasticity of nano-metallic laminates. J. Mech. Phys. Solid. 173, 105187. https://doi.org/10.1016/j.jmps.2022.105187.

Zhang, C., Wang, Y., Yang, Z., Guo, Y., Bingjun, D., 2004. Microstructure and properties of vacuum induction melted CuCr25 alloys. J. Alloys Compd. 366, 289–292. https://doi.org/10.1016/j.jallcom.2003.07.001.